Biomedical Signal Processing and Control 3 (2008) 312–318

Contents lists available at ScienceDirect

Biomedical Signal Processing and Control

journal homepage: www.elsevier.com/locate/bspc

Morphological measurement of localized temperature increase amplitudes in breast infrared thermograms and its clinical application

Xianwu Tang [a], Haishu Ding [a,*], Yun-e Yuan [b], Qing Wang [b]

[a] Department of Biomedical Engineering, Tsinghua University, Beijing 100084, China
[b] Institute of Basic Medical Science in PLA General Hospital, Beijing 100853, China

ARTICLE INFO

Article history:
Received 12 October 2007
Received in revised form 16 March 2008
Accepted 21 April 2008
Available online 15 August 2008

Keywords:
Infrared thermography
Localized temperature increase
Mathematical morphology
Breast cancer detection
Screening

ABSTRACT

Malignant tumors will cause localized temperature increases (LTI) on breast surface which show as spot or vascular patterns in breast infrared thermograms. Thermographic detection of breast cancer now primarily depends on the visual analysis of these patterns by physicians, which is hard to provide objective and quantitative results. In this paper, we propose a new criterion of breast cancer detection and the method of its realization as follows: (1) surface temperature distribution of a healthy breast usually exhibits a gentle variation which is background. (2) Localized surface temperature of a carcinomatous breast will increase on the basis of the above background which is LTI. (3) The carcinomatous possibility is proportional to the LTI maximum (amplitude) of the suspicious focus region. (4) The LTI amplitude can be measured through morphological signal processing. According to the above conception, we obtained LTI amplitudes of 117 breast disease patients including 70 benign cases and 47 malignant cases. The optimal LTI amplitude threshold for breast cancer detection is determined as 1 °C from the ROC (receiver operating characteristic) curve based on the rule of Youden's index maximization. 44 cases were screened out from 47 breast cancer patients under this threshold. High sensitivity 93.6% and high NPV (negative predictive value) 91.2% demonstrate the value of this method on preliminary screening of breast cancer. High FPR (false-positive rate) 55.7% suggests that it is better to apply this method together with others.

1. Introduction

Infrared thermography is a promising technology for breast cancer detection [1]. It uses an infrared camera or scanner to detect the natural thermal radiation at wavelengths between 0.8 μm and 1.0 mm emitted from the human body and obtains an image recording the surface skin temperature distribution of that body which is also called infrared thermogram [2]. When a malignant tumor occurs in a breast, it will cause prominent localized increase of breast surface skin temperature for its high metabolic activity and blood perfusion [2–6]. The LTI shows as spot or vascular pattern in a breast infrared thermogram which is also called heat pattern. Breast cancer can be detected through the visual analysis of heat patterns by physicians [2,7–9].

The Food and Drug Administration (FDA), Bureau of Medical Devices has already confirmed thermographic detection of breast cancer [10]. Jones [2] considered thermography particularly valuable for early breast cancer detection in the recent reappraisal of its usage in medicine. Keyserlingk et al. [11] reported that the average size of tumors undetected by thermography is 1.28 cm, while 1.66 cm by mammography. Ng et al. [9] also mentioned that the result of thermography could be corrected 8–10 years before mammography can detect a mass. Thermography is non-contact, noninvasive, innocuous, considerably cheap and risk-free to both patients and physicians for without ionizing radiation. It is a proper choice for annual routine medical check-up of breast cancer [9].

Though thermographic detection of breast cancer now primarily depends on the visual analysis of thermograms by physicians, computer-assisted analysis of thermograms for breast cancer detection recently has drawn much attention [1,6–9,12–21]. Some related research works of this field are focused on the asymmetry analysis of the temperature distribution of bilateral breast regions [9,13]. Ng et al. carried out comprehensive research works on the application of computer simulation [6,15,16] and artificial neural network [17–21] in computerized thermographic detection of breast cancer. In this paper, we propose two steps to realize the breast cancer detection. Firstly, visually find out the suspicious focus regions in breast infrared thermograms. Secondly, measure

* Corresponding author.
E-mail address: dhs-dea@mail.tsinghua.edu.cn (H. Ding).

1746-8094/$ – see front matter © 2008 Elsevier Ltd. All rights reserved.
doi:10.1016/j.bspc.2008.04.001

the LTI amplitudes of these regions with morphological approaches and use the measurement results as a criterion of breast cancer detection. The feasibility of the above conception has been preliminarily verified in 117 breast disease patients.

2. Methods

2.1. LTI in breast infrared thermograms

A breast infrared thermogram of a breast cancer patient is displayed in gray scale in Fig. 1. The brighter pixels have higher temperature values. There is a vascular heat pattern in the white framed box of Fig. 1 formed by the LTI in the breast region. If the temperature value of each pixel in a thermogram is viewed as an elevation, the whole thermogram can be viewed as a topographic surface. Fig. 2 shows the imaginary topographic surface of the white box region in Fig. 1. From Fig. 2, a clear characteristic of breast cancer thermogram which is the LTI superposing on the background temperature distribution with large-scale slow variation can be found.

The key of measuring LTI amplitude is to obtain the background temperature distribution of the LTI region. If it can be obtained, the temperature increase value of each pixel in the LTI region can be calculated as its temperature minus the corresponding background temperature. The maximum of temperature increase values of all the pixels is defined as the LTI amplitude.

In geography, uplift degree of a mountain can be reflected more by its localized elevation increase amplitude (peak elevation minus its plateau elevation) than the peak absolute elevation. For a thermogram, prominence of LTI can be better reflected by the LTI amplitude than the absolute temperature value of the LTI region. Since the occurrence of breast cancer will cause prominent LTI, the higher LTI amplitude can indicate a higher carcinomatous possibility.

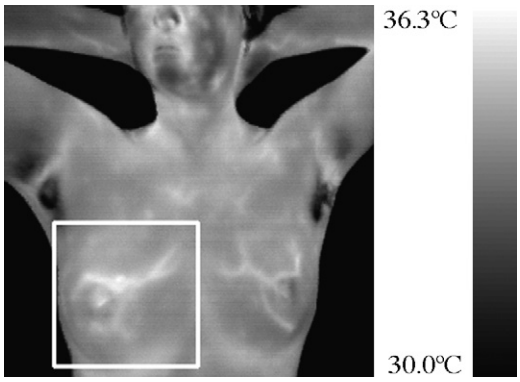

Fig. 1. Infrared thermogram of a breast cancer patient with a vascular heat pattern in the white box.

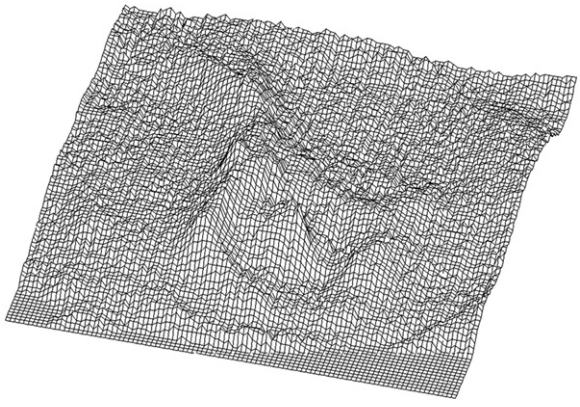

Fig. 2. Imaginary topographic surface of the white box region in Fig. 1.

2.2. Principles of morphological approaches

Mathematical morphology is a popular signal processing technology in image processing [22]. The common morphological operators include erosion, dilation, opening and top-hat, etc. Processes of these operators are implemented with a geometric template such as line or disc which is called structuring element (SE) [23]. When the template origin is placed on a pixel in the processed gray-scale image, the template determines a small domain. The erosion result of the pixel is defined as the minimum of the gray values of all the pixels in the domain, while the dilation result is the maximum. Let the template origin traverse all the pixels in the image and perform the min or max operation in the determined domain, the erosion or dilation result of the whole image can be obtained. Performing dilation on the erosion result leads to the opening result. Subtracting the opening result from the original image leads to the top-hat result.

An example of 1-d (one-dimensional) gray value sequence f will be used to describe how to implement extraction and amplitude measurement of localized gray value increases (LGI) through erosion, dilation, opening and top-hat:

(1) Description of f. f is shown as a strip of 20 pixels with different gray values in Fig. 3a. Its gray value distribution is shown in Fig. 3b. The horizontal axis is point number and the vertical axis is gray value. In Fig. 3b two peaks can be found (left and right) which are formed by LGI in f. Their center positions are point 5 and point 15. The two peaks are chosen as the measured regions.
(2) Choose the proper SE. The line SE B with 7 points is adopted and its origin is the midpoint. Move the SE from left to right and let its origin on each point of f during the process.
(3) Perform erosion on f. Suppose the SE origin is on the point 5. The domain determined by the SE includes 7 points {2, 3, 4, 5, 6, 7, 8}. Their gray values are {6, 6, 9, 10, 8, 6, 6}. The erosion result of point 5 is 6, the minimum of all the gray values in the domain. The erosion result $\varepsilon_B(f)$ is shown in Fig. 3c.
(4) Perform opening on f. The opening result $\gamma_B(f)$ is $\delta_B(\varepsilon_B(f))$, the dilation of the erosion result $\varepsilon_B(f)$. The peaks formed by LGI are cut off after opening as shown in Fig. 3d. The opening result $\gamma_B(f)$ has a gentler gray value variation when compared with f. It is approximately taken as the background. It should be noted that though its gray values variate gently, they are not constant.
(5) Perform top-hat on f. The gray value increase of each point in f is obtained through subtracting its approximate background value $\gamma_B(f)$ from f, which is also its top-hat result $\mathrm{TH}_B(f)$. The extraction of LGI is implemented through top-hat.
(6) Measure LGI amplitudes. The morphological measurement results of LGI amplitudes in f can be obtained through max operation on two peak regions of extracted gray value increases in Fig. 3e. They are 4 (left) and 6 (right), respectively. The results indicate that the morphological measurement reflect the gray value increases on the basis of the background, not the absolute gray value height of the peaks which are 10 (left) and 9 (right).
(7) Determination of the SE size. In fact, a series of line SEs with the widths $2k + 1$ ($k = 1, 2, 3, \cdots$) is tried to determine the proper width of the line SE. The results of opening and top-hat are denoted as $\gamma_k(f)$ and $\mathrm{TH}_k(f)$. Fig. 4 shows the results at width 3 which are $\gamma_1(f)$ and $\mathrm{TH}_1(f)$. Fig. 5 shows the results at width 5

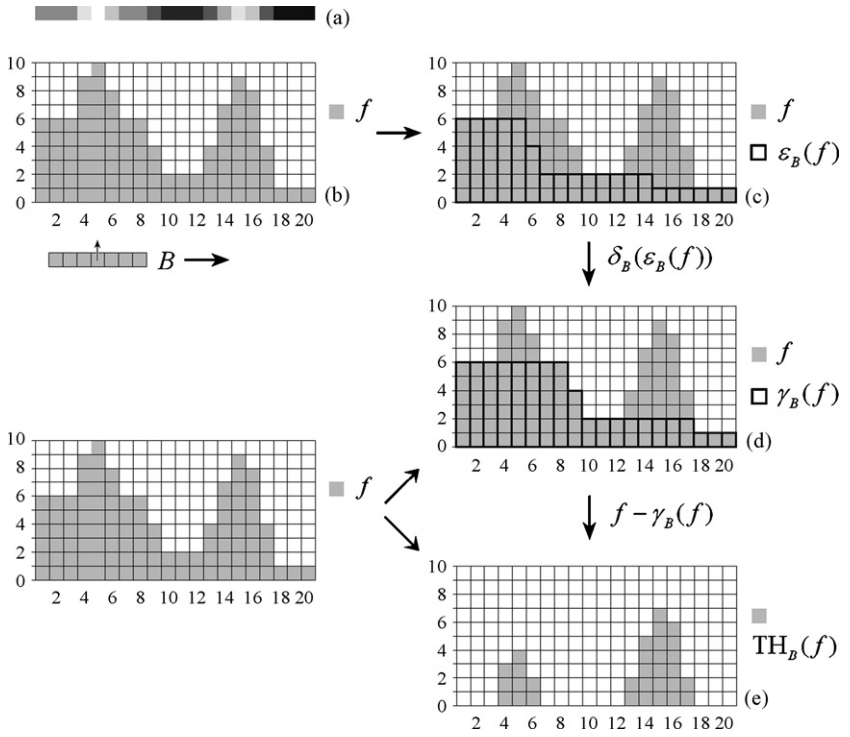

Fig. 3. Principles of morphological measurement of LGI amplitudes in the 1-d gray value sequence f. (a) Gray strip of gray value sequence f. (b) Gray value distribution of f. (c) Erosion result $\varepsilon_B(f)$. (d) Opening result $\gamma_B(f)$. (e) Top-hat result $\mathrm{TH}_B(f)$.

which are $\gamma_2(f)$ and $\mathrm{TH}_2(f)$. The results at width 7 have already been shown in Fig. 3. The results at widths 9, 11, and 13 are the same as the ones at width 7.

Maragos mentioned in [24] that opening can cut off peaks and form plateaus. As shown in Figs. 4 and 5, the peaks formed by LGI are gradually cut off and the plateaus close to the background are gradually formed with the line SE width increasing from 3 to 5. When the line SE width increases to a proper value 7, the opening result can be considered very close to the background as shown in Fig. 3d. So the opening result at width 7 is taken as the approximated background. After that, even the line SE width is increased to 9, 11, and 13, the opening result has no change and keeps the same as the one at width 7, for the peaks are completely cut off and the opening has no effect on the plateaus close to the background. It also indicates that the opening result at width 7 is a proper choice for the approximate background.

It can be found that opening can extract the background from f as shown in Fig. 3. Though gray values of the background variate gently, they still keep the trend of variating from the higher plateau to the lower plateau. The background gray values of different positions can be different. Although the left peak has a higher gray value (10), its LGI amplitude is not big and its morphological measurement result is 4, because it is located on the higher plateau and has a higher background gray value. While the right peak has higher LGI amplitude whose morphological measurement result is 6 though its gray value (9) is lower. Because it is located on the lower plateau and has a lower background gray value. Morpho-

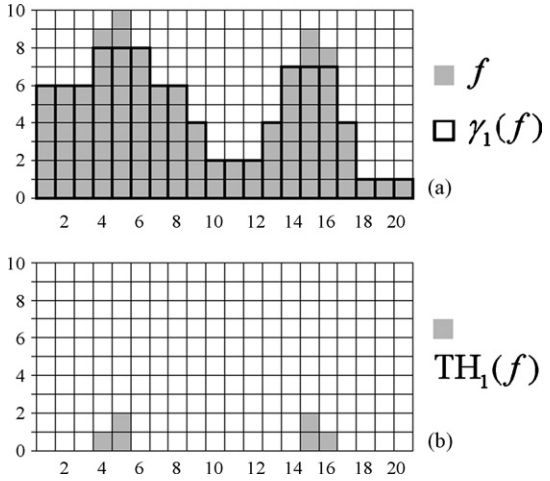

Fig. 4. The results of opening and top-hat at width 3 which are $\gamma_1(f)$ (a) and $\mathrm{TH}_1(f)$ (b).

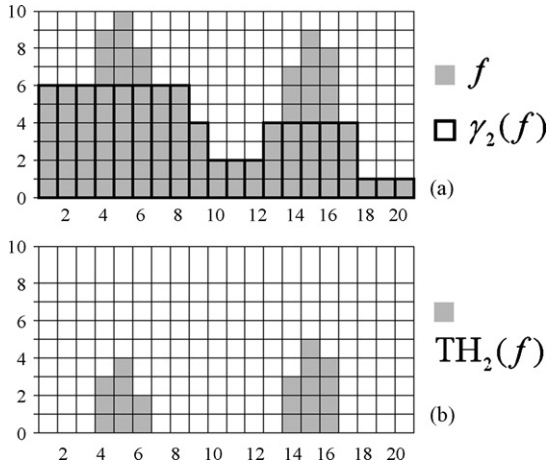

Fig. 5. The results of opening and top-hat at width 5 which are $\gamma_2(f)$ (a) and $\mathrm{TH}_2(f)$ (b).

logical measurement results reflect the actual situations of LGI: the one has higher gray value may not have higher LGI amplitude.

This characteristic of morphological approaches is the one right needed in the measurement of LTI amplitudes. Though there is no LTI on the healthy woman breast surface, but its temperature distribution is not constant. The upper half of the healthy woman breast is warmer than the lower half possibly for more vessels being in the upper half of the breast [25]. There also exists a background temperature variation like the higher plateau to the lower plateau in Fig. 3. When measuring LTI amplitudes in different positions of the breast region of each breast disease patient, different background temperature values need to be extracted. The above morphological approaches provide a method of extracting background temperature so that breast cancer can be better detected by the LTI amplitude.

2.3. Measurement of LTI amplitudes

According to the principles of morphological measurement of LGI amplitudes in a 1-d gray value sequence in Section 2.2, measurement of LTI amplitudes in breast infrared thermograms with morphological approaches can be implemented. We will describe the process on the breast thermogram example of Fig. 6.

(1) Choose the region for measurement. As shown in Fig. 6, a physician can draw the edge of the region where measurement of LTI amplitude is needed.
(2) Choose the proper SE. The disc SE is chosen for the breast thermogram is 2-dimensional. In order to determine the proper radius of the disc SE, the openings using a series of disc SEs with radii from small to big are performed on the breast thermogram. If the opening result at each radius is taken as the approximate background, the temperature increase value of each pixel in the measured region can be obtained. The maximum of temperature increase values of all the pixels in the region is the morphological measurement result of LTI amplitude at each radius.

When the radius changes from small to big, the opening will cut off more and more LTI part and the morphological measurement result will also increase. The practical process result reveals that from the beginning of some radius the morphological measurement result will keep unchanged as the opening result is very close to the background. We will illustrate it through the process of a practical breast thermogram in Fig. 6. For the data of Fig. 6, the curve of the morphological measurement result of LTI amplitude changing with the disc SE radius is obtained which is shown in Fig. 7. The unit of LTI amplitude is °C and the radius unit is pixel. It can be found that from the beginning of radius 13 pixels the morphological measurement result keeps 1.3 °C unchanged in the following 3 radii.

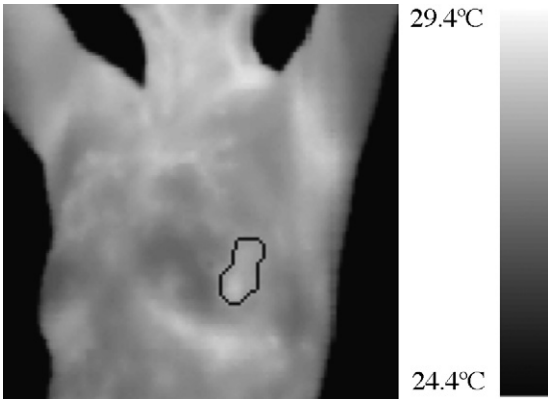

Fig. 6. Breast infrared thermogram and edge of the measured region.

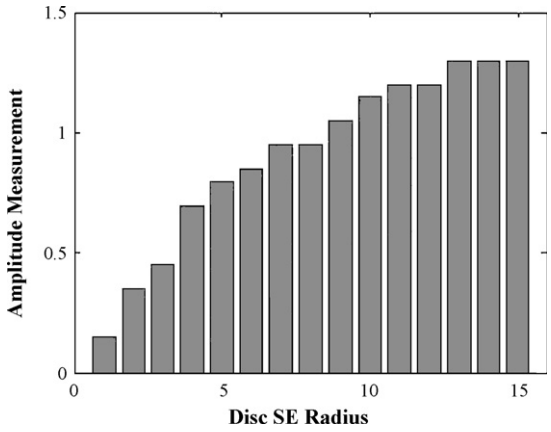

Fig. 7. The curve of morphological measurement result of LTI amplitude versus disc SE radius.

In this paper, breast infrared thermograms of 117 breast disease patients are collected to form the data set which will be introduced in Section 3.1. Breast thermogram in Fig. 6 is from one of the 117 patients. In the process of breast thermograms of these patients, it is found that if the result keeps unchanged for 3 radii, the result can be considered stable and meaningful. Thus it is defined as the final result.

Through Fig. 6, it can be found that though the region is partially in the lower half of the breast and its maximum temperature is not high, its morphological measurement result of LTI amplitude is as high as 1.3 °C for the low background temperature values. This example also indicates that breast cancer can be better detected by the LTI amplitude through measurement with morphological approaches. Large process results show that the approach from this example is also applicable for the breast thermograms from other patients.

(3) If there are many measured regions in the patient thermogram, the maximum of the measurement results of all the regions is taken as the LTI amplitude of the thermogram.

3. Results

3.1. Data set and morphological measurement results of LTI amplitudes

The infrared thermography system TSI-21 from BIOYEAR Inc. [26] is used. The temperature resolution of this system is 0.05 °C at 30 °C and the acquired image size is 256 pixels × 256 pixels. The preoperative breast infrared thermograms of 117 breast disease patients are collected under the recommended conditions in [9,12] in the PLA General Hospital. The 117 cases are confirmed to be 70 benign and 47 malignant through pathological examination. The morphological measurement results of LTI amplitudes of 70 benign cases and 47 malignant cases are shown in Fig. 8a and b.

3.2. Difference between benign and malignant cases in LTI amplitude

In order to determine the significance of the difference between benign and malignant cases in the LTI amplitude, t test is carried out. The number of benign cases n_1 is 70. The mean μ_1 and the standard deviation σ_1 of the LTI amplitude of benign cases are 1.18

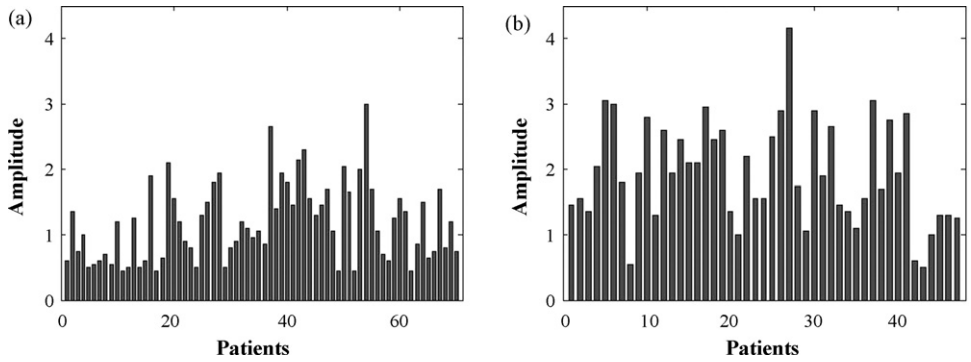

Fig. 8. Morphological measurement results of LTI amplitudes of benign cases (a) and malignant cases (b).

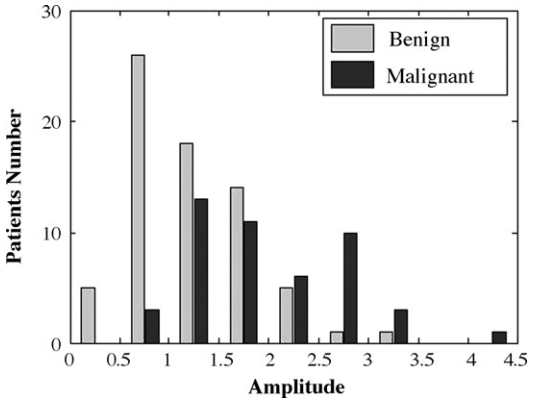

Fig. 9. Histogram of LTI amplitudes of benign and malignant cases in all the ranges.

and 0.59 °C, respectively. The number of malignant cases n_2 is 47. The mean μ_2 and the standard deviation σ_2 of the LTI amplitude of malignant cases are 1.94 and 0.79 °C, respectively. The t value is calculated as [27]:

$$t = \frac{|\mu_1 - \mu_2|}{S\sqrt{\frac{1}{n_1} + \frac{1}{n_2}}}, \quad S = \sqrt{\frac{(n_1 - 1)\sigma_1^2 + (n_2 - 1)\sigma_2^2}{n_1 + n_2 - 2}}.$$

The calculation result of t value is 5.98. When the significance level p is set as 0.001, the critical value of t with the degrees of freedom 115 ($n_1 + n_2 - 2$) is written as $t_{115,0.001}$. It can be obtained from the ordinary t table which is 3.16. The result of $t > t_{115,0.001}$ suggests that there is a significant difference between benign and malignant cases in the LTI amplitude.

The distribution of LTI amplitudes of benign and malignant cases in all the ranges is shown in Fig. 9 and Table 1. It can be found that the higher LTI amplitude indicates a higher possibility of being cancer. When the amplitude range is 0–1.00 °C, there are 3 malignant cases and 31 benign cases. The proportion of malignant cases and benign cases are 8.8% (3/34) and 91.2% (31/34), respectively. When the amplitude range is 1.00–2.50 °C, there are 30 malignant cases and 37 benign cases. The proportion of malignant cases and benign cases are 44.8% (30/67) and 55.2% (37/67), respectively. When the amplitude range is ≥2.50 °C, there are 14 malignant cases and 2 benign cases. The proportion of malignant cases and benign cases are 87.5% (14/16) and 12.5% (2/16), respectively.

3.3. Detecting breast cancer by LTI amplitude

When a LTI amplitude threshold is set for breast cancer detection, patients with LTI amplitudes not lower than the threshold have positive results while the others have negative results. The patients can be categorized into 4 classes: true positive (TP), false negative (FN), false positive (FP) and true negative (TN). Their definitions are shown in Table 2.

Some statistical parameters to evaluate the performance of LTI amplitude in breast cancer detection [9] can be calculated from Table 2:

Sensitivity: TP/(TP + FN).
Specificity: TN/(TN + FP).
False-positive rate (FPR): 1 − specificity.
Youden's index [28]: sensitivity − FPR.
Positive predictive value (PPV): TP/(TP + FP).
Negative predictive value (NPV): TN/(TN + FN).

Sensitivity reflects the capability of detecting breast cancer while specificity reflects the capability of detecting benign disease. Youden's index reflects the total capability of detecting cancer and benign disease. PPV reflects the malignant possibility of positive result while NPV reflects the benign possibility of negative result.

When the LTI amplitude thresholds are set from 0.5 to 3.5 °C with 0.5 °C interval, 7 pairs of sensitivity and FPR can be obtained. If sensitivity is plotted on the y axis and FPR on the x axis, these pairs of sensitivity and FPR are the points marked with circles in Fig. 10. If the starting point (0, 0) and the ending point (1, 1) are added and these points are connected with lines, a curve of sensitivity versus FPR which is called ROC curve [29] is obtained.

The ideal result of detection is that the sensitivity is 1 and the FPR is 0. From the ROC curve in Fig. 10, it can be found that when the threshold decreases sensitivity will increase to 1 but FPR will also increase to 1. At the same time, when the threshold increases FPR will decrease to 0 but sensitivity will also decrease to 0. The

Table 1
Distribution of LTI amplitudes of benign and malignant cases in all the ranges

Amplitude (°C)	0–0.50	0.50–1.00	1.00–1.50	1.50–2.00	2.00–2.50	2.50–3.00	≥3.00
Malignant	0	3	13	11	6	10	4
Benign	5	26	18	14	5	1	1

Note: Range 0–0.50 does not include 0.50 and the other ranges are all the same.

Table 2
Contingency table

	Benign	Malignant	Total
Negative	TN	FN	TN + FN
Positive	FP	TP	FP + TP
Total	TN + FP	FN + TP	

Youden's index can be used to evaluate the total result of a threshold. The optimal LTI amplitude threshold can be determined based on the rule of Youden's index maximization. Youden's indexes of all thresholds are shown in Fig. 11. The maximum of Youden's index 0.38 occurs at threshold 1 °C, and 1 °C is set as the optimal threshold. According to Table 1, TN, FP, FN and TP under the optimal threshold 1 °C are 31, 39, 3 and 44. The sensitivity is 93.6% (44/47) and the FPR is 55.7% (39/70). Youden's index is 0.38. The PPV is 53.0% (44/83) and the NPV is 91.2% (31/34). Detecting breast cancer by LTI amplitude has the characteristics of high sensitivity, high NPV and high FPR.

The details of 3 undetected breast cancer cases are listed in Table 3. The 3 cases are all advanced cancer, where 2 cases are advanced ductal carcinoma and 1 case is advanced medullary carcinoma. When the cancer is in the advanced stage, the metabolic activity of tumor will descend [4] and the LTI will not be prominent. Furthermore, 2 cases are very old (≥60) and their basal metabolic rates are low. The LTI amplitudes of the 3 case are only 0.50–0.60 °C. It indicates that detecting breast cancer by LTI amplitude may be insensitive to the advanced cancer especially the old ones.

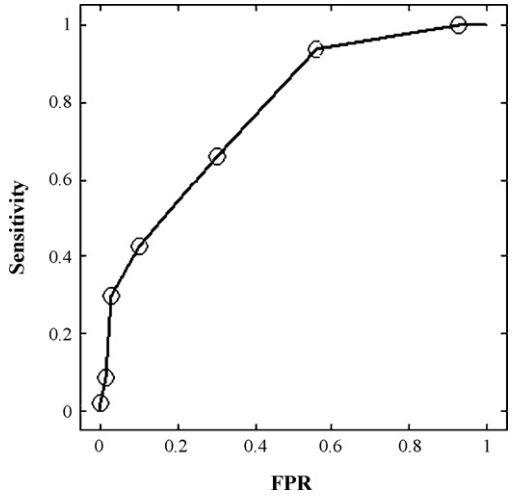

Fig. 10. ROC curve.

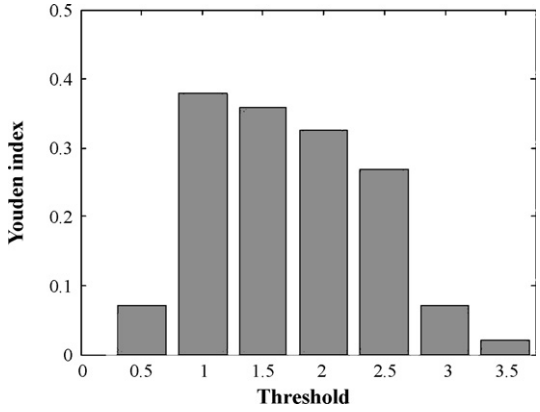

Fig. 11. Youden's indexes of all thresholds.

Table 3
Details of 3 undetected breast cancer cases

Case	Age	Cancer type	Stage	Amplitude (°C)
1	68	Ductal carcinoma	Advanced	0.55
2	45	Ductal carcinoma	Advanced	0.60
3	60	Medullary carcinoma	Advanced	0.50

Table 4
Details of 2 detected early breast cancer cases

Case	Age	Cancer type	Stage	Amplitude (°C)
1	24	Ductal carcinoma	Early	2.75
2	27	Ductal carcinoma	Early	2.85

Among the detected cases, we find 2 young and early breast cancer cases and their details are listed in Table 4. The 2 cases have very high LTI amplitudes (>2.5 °C). It may be related with the high basal metabolic rate of young woman and the high metabolic activity and blood perfusion of early cancer [4]. It indicates that early detection of breast cancer may be achieved by LTI amplitude.

3.4. Application of LTI amplitude in breast cancer detection

There occurs a high FPR 55.7% in the breast cancer detection by LTI amplitude in the 117 breast disease cases. It indicates that LTI amplitude may not have good specificity. Many factors including benign breast diseases may cause LTI. LTI is not a specific sign of the occurrence of breast cancer [2,12]. But high sensitivity 93.6% and high NPV 91.2% indicate that LTI amplitude can be parameter for breast cancer screening. Thermography is harmless, cheap and also can achieve early detection of breast cancer. Thermography is very suitable for screening breast cancer in a large population. LTI amplitude may help physicians decrease the possibility of missing breast cancer cases in screening through adopting the parameter of LTI amplitude.

4. Conclusion

In this paper, we proposed the morphological measurement of LTI amplitudes in breast infrared thermograms and the clinical application of measurement results in breast cancer detection. Through applying morphological approaches, we obtained LTI amplitudes of 117 breast disease patients including 70 benign cases and 47 malignant cases. We find a significant difference ($p < 0.001$) between benign and malignant cases in the LTI amplitude through t-test. The patients with higher LTI amplitudes have higher carcinomatous possibility. We determine the optimal LTI amplitude threshold of 1 °C for breast cancer detection from the ROC curve based on the rule of Youden's index maximization. Under the optimal threshold, 44 cases are detected from 47 breast cancer cases. The 3 undetected cancer cases are all advanced cancer and 2 cases are from very old patients. It indicates that breast cancer detection by LTI amplitude may be insensitive to the advanced breast cancer and especially to the aged case. There are 2 young and early cancer cases among the detected cases. It indicates that early detection of breast cancer may be achieved by LTI amplitude. At the same time, the high FPR 55.7% indicates that LTI amplitude may not have good specificity. The high sensitivity 93.6% and high NPV 91.2% demonstrate that LTI amplitude can be used as parameter for breast cancer screening. It can help physicians decrease the possibility of missing breast cancer cases.

It has already been applied in the breast cancer screening by thermography in the PLA General Hospital.

References

[1] J.F. Head, R.L. Elliott, Infrared imaging: making progress in fulfilling its medical promise, IEEE Eng. Med. Biol. Mag. 21 (2002) 80–85.
[2] B.F. Jones, A reappraisal of the use of infrared thermal image analysis in medicine, IEEE Trans. Med. Imaging 17 (6) (1998) 1019–1027.
[3] M.M. Osman, E.M. Afify, Thermal modelling of the malignant woman's breast, Trans. ASME J. Biomech. Eng. 110 (1988) 269–276.
[4] N.M. Sudharsan, E.Y.K. Ng, S.L. The, Surface temperature distribution of a breast with/without tumor, Int. J. Comput. Meth. Biomech. Biomed. Eng. 2 (1999) 187–199.
[5] E.Y.K. Ng, N.M. Sudharsan, An improved three-dimensional direct numerical modelling and thermal analysis of a female breast with tumour, Int. J. Eng. Med. 215 (H4) (2001) 25–37.
[6] E.Y.K. Ng, N.M. Sudharsan, Numerical computation as a tool to aid thermographic interpretation, J. Med. Eng. Technol. 25 (2001) 53–60.
[7] J.R. Keyserlingk, P.D. Ahlgren, E. Yu, N. Belliveau, M. Yassa, Functional infrared imaging of the breast, IEEE Eng. Med. Biol. Mag. 19 (2000) 30–41.
[8] J.F. Head, F. Wang, C.A. Lipari, R.L. Elliott, The important role of infrared imaging in breast cancer, IEEE Eng. Med. Biol. Mag. 19 (2000) 52–57.
[9] E.Y.K. Ng, L.N. Ung, F.C. Ng, Statistical analysis of healthy and malignant breast thermography, J. Med. Eng. Technol. 25 (2001) 253–263.
[10] S.K. Moore, Better breast cancer detection, IEEE Spectr. 38 (2001) 50–54.
[11] J.R. Keyserlingk, P.D. Ahlgren, E. Yu, N. Belliveau, Infrared imaging of the breast: initial reappraisal using high resolution digital technology in 100 successive cases of stage I and II breast cancer, Breast J. 4 (1998) 245–251.
[12] B.F. Jones, P. Plassmann, Digital infrared thermal imaging of human skin, IEEE Eng. Med. Biol. Mag. 21 (2002) 41–48.
[13] H. Qi, W. Snyder, J.F. Head, R.L. Elliott, Detecting breast cancer from infrared images by asymmetry analysis, Proc. 22nd Annu. Conf. IEEE Engineering in Medicine and Biology Society, July 23–28, 2000, Chicago, IL.
[14] E.Y.K. Ng, Y. Chen, L.N. Ung, Computerized breast thermography: study of image segmentation and temperature cyclic variations, J. Med. Eng. Technol. 25 (1) (2001) 12–16.
[15] E.Y.K. Ng, N.M. Sudharsan, Effect of blood flow, tumour and cold stress in a female breast: a novel time-accurate computer simulation, Int. J. Eng. Med. 215 (H4) (2001) 393–404.
[16] E.Y.K. Ng, N.M. Sudharsan, Numerical modelling in conjunction with thermography as an adjunct tool for breast tumour detection, BMC Cancer 4 (17) (2004) 1–26.
[17] E.Y.K. Ng, S.C. Fok, Y.C. Peh, F.C. Ng, L.S.J. Sim, Computerized detection of breast cancer with artificial intelligence and thermograms, J. Med. Eng. Technol. 26 (4) (2002) 152–157.
[18] E.Y.K. Ng, S.C. Fok, A framework for early discovery of breast tumor using thermography with artificial neural network, Breast J. 9 (4) (2003) 341–343.
[19] E.Y.K. Ng, E.C. Kee, Advanced integrated technique in breast cancer thermography, J. Med. Eng. Technol. 17 (2007) 1–12.
[20] T.Z. Tan, C. Quek, G.S. Ng, E.Y.K. Ng, A novel cognitive interpretation of breast cancer thermography with complementary learning fuzzy neural memory structure, Expert Syst. Appl. 33 (3) (2007) 652–666.
[21] E.Y.K. Ng, Improved sensitivity and specificity of breast cancer thermography, in: M.A. Hayat (Ed.), Cancer Imaging, Elsevier, USA, 2007, pp. 439–448.
[22] J. Serra, Image Analysis and Mathematical Morphology, Academic, New York, 1982.
[23] J. Goutsias, H. Heijmans, Fundamenta morphologicae mathematicae, Fundamenta Informaticae 41 (200) (2000) 1–31.
[24] P. Maragos, Pattern spectrum and multiscale shape representation, IEEE Trans. Pattern Anal. Mach. Intell. 11 (1989) 701–716.
[25] M.M. Osman, E.M. Afify, Thermal modelling of the normal woman's breast, Trans. ASME J. Biomech. Eng. 106 (1984) 123–130.
[26] Z.Q. Liu, C. Wang, Method and apparatus for thermal radiation imaging, United States Patent 6023637, 2000.
[27] W.S. George, G.C. William, Statistical Methods, The Iowa State University Press, 1980.
[28] W.J. Youden, Index for rating diagnostic test, Cancer 3 (1950) 3–32.
[29] N.A. Obuchowski, Receiver operating characteristic curves and their use in radiology, Radiology 229 (2003) 3–8.